Energy Reports 8 (2022) 4274–4281

Contents lists available at ScienceDirect

Energy Reports

journal homepage: www.elsevier.com/locate/egyr

Research paper

Heat-pipe-based tunable multimode horizontal thermal rectifier

Zhanxiao Kang, Jintu Fan *

Institute of Textiles and Clothing, The Hong Kong Polytechnic University, Kowloon, Hong Kong, China

ARTICLE INFO

Article history:
Received 22 January 2022
Received in revised form 2 March 2022
Accepted 8 March 2022
Available online xxxx

Keywords:
Horizontal thermal rectifier
Superhydrophilic/superhydrophobic surface
Thermal valve
Thermal energy management

ABSTRACT

A heat-pipe-based multimode thermal rectifier, easily scalable for advanced thermal energy management in industrial applications (e.g., waste heat recovery, solar energy application and building energy management), is proposed for horizontal heat transport. The thermal rectifier is composed of a copper tube loop having a superhydrophilic section and a superhydrophobic section. The thermal rectification effect is achieved by the differences of the superhydrophilic and superhydrophobic sections in surface evaporation/condensation and wicking characteristics, when they are exposed to heating or cooling. Meanwhile, a valve is incorporated in the vapor channel to control the switch status of the hot vapor flow. Experiments with such a thermal rectifier showed that a maximum thermal rectification ratio of 4.18 could be reached at the heat flux of 3222 W/m^2, whereas a higher rectification ratio (up to 5.78) could even be achieved when forward and reversed heat transfer are at different heating temperatures in real applications. Besides, the forward thermal conductivity could reach 623 W/(m·K) for efficient waste heat harvest. In addition, the thermal rectification ratio, as well as the heating mode, can be tuned by the status of the valve in the tube loop to satisfy the complex requirement in practical applications.

1. Introduction

Fossil energy occupies about 85% of the total energy consumption in the world, which not only produces much pollution but also leads to global warming threatening the living environment of mankind. Taking full advantage of the waste heat from industries could decrease fossil energy consumption and reduce greenhouse gas emissions. Hence, many technologies (Liu et al., 2006; Garimella, 2012; Crane and Jackson, 2004; Mahajan et al., 2017; Mahmoudi et al., 2018) have been developed for waste heat recovery, such as waste heat boilers, air preheaters, water heaters, and heat pipes (Jouhara et al., 2018; Hervás-Blasco et al., 2019; Kang et al., 2021; Kang and Wang, 2018), which perform well for stable waste heat. However, the waste heat generation is generally unstable in many circumstances, which reduces the working efficiency of the existing waste heat recovery systems (Wang and Wu, 2005). Besides, solar energy is also a type of unstable energy that constrains its widespread applications (Rivera and Rivera, 2003). A thermal rectifier has lower thermal resistance in one direction than that in the opposite direction, which is highly desirable for unstable waste heat recovery and solar energy harvest. For instance, a thermal rectifier can be used to harvest waste heat to obtain domestic hot water but preserve the heat of the hot water during the interval of the waste heat generation. In addition, the thermal rectifier also could control the heat transport between the building's indoor and outdoor environments, which is beneficial to reducing the building energy consumption for air conditioning.

In general, the solid bi-material systems consisting of two solid components, which have highly temperature-dependent thermal conductivities and matching properties between the phonon bands at the junction of the lattices, could perform a thermal rectification effect (Hu et al., 2008; Pal and Puri, 2014; Hu et al., 2006; Ordonez-Miranda et al., 2018; Hamaoui et al., 2019; Shrestha et al., 2020). Takeuchi (2014) reported a solid thermal rectifier fabricated by Al-based icosahedral quasi-crystal (IQC) and the highest rectification ratio was only 1.65. Zhang and Luo (2015) proposed a thermal diode based on different phases of polyethylene nanofiber and its thermal rectification factor was up to 1.2 due to the phase-dependent thermal conductivity of the polyethylene nanofibers. Nonetheless, the interface property of the solid thermal rectifier is difficult to control precisely, which leads to a great challenge for the fabrication of the solid-state thermal rectifier. Furthermore, solid thermal rectifiers generally have low rectification ratios and small forward thermal conductivities, and therefore they are difficult to be used for industrial waste heat harvesting.

For practical thermal applications, Villeneuve et al. (2017) reported a thermal diode composed of an array of paralleled-located air gaps, through which heat could transport from bottom to top by natural convection at the bottom heating mode, while

* Corresponding author.
E-mail address: jin-tu.fan@polyu.edu.hk (J. Fan).

https://doi.org/10.1016/j.egyr.2022.03.042

Nomenclature

A	total cross section area of the top and bottom tubes (m^2)
k	equivalent thermal conductivity (W/(m·K))
L	distance between the heating and cooling sections of the thermal rectifier (m)
q	input heat flux from the heating tube surface (W/m^2)
Q	heating power (W)
ΔQ	heating power uncertainty (W)
R	thermal resistance (K/W)
ΔR	thermal resistance uncertainty (K/W)
R_r	thermal resistance during reversed heating (K/W)
ΔR_r	uncertainty of the reversed thermal resistance (K/W)
R_f	thermal resistance during forward heating (K/W)
ΔR_f	uncertainty of the forward thermal resistance (K/W)
T_1	bottom temperature of the superhydrophilic tube (° C)
T_2	middle temperature of the superhydrophilic tube (° C)
T_3	top temperature of the superhydrophilic tube (° C)
T_4	bottom temperature of the superhydrophobic tube (° C)
T_5	middle temperature of the superhydrophobic tube (° C)
T_6	top temperature of the superhydrophobic tube (° C)
T_{bottom}	bottom temperature of the cooling tube (° C)
T_c	average temperature of the cooling tube (° C)
ΔT_c	average temperature uncertainty of the cooling tube (° C)
T_h	average temperature of the heating tube (° C)
ΔT_h	average temperature uncertainty of the heating tube (° C)
T_{middle}	middle temperature of the cooling tube (° C)
T_{top}	top temperature of the cooling tube (° C)

Greek symbols

ε_R	measurement error of thermal resistance (-)
ε_φ	measurement error of rectification ratio (-)
φ	thermal rectification ratio (-)
$\Delta\varphi$	uncertainty of thermal rectification ratio (-)

Abbreviations

FCRO	forward heating with closed valve and reversed heating with open valve
FORC	forward heating with open valve and reversed heating with closed valve

the heat transport was blocked due to the low thermal conductivity of air at the top heating mode. Chen et al. (1998) studied a thermal rectifier based on thermosiphon, in which heat preferred to transport from the lower cavity to the higher tank through natural convection, whereas the inverse heat transport was restricted due to the low thermal conductivity of water. Zhang et al. (2020) introduced a thermosiphon loop to the solar water heating system, which could reduce the water heat loss at night time. Besides, Azad (2008) investigated a gravity assisted heat pipe solar collector for hot water production. Moreover, Pei et al. (2019) proposed a heat-pipe-based thermal rectifier to cool permafrost thaw by the ambient cool air due to its one-way heat transfer features from bottom to top. Furthermore, the heat pipes with an inclination angle (Susheela and Sharp, 2001; Varga et al., 2002) embedded in the wall were also applied for the advanced thermal management of buildings due to their thermal diode effect.

In addition, Pugsley et al. (2019) and Edalatpour et al. (2020) proposed the liquid–vapor thermal diode with an EPDM (Ethylene Propylene Diene Monomer) gasket sealing the device, and the rectification ratio was more than 15 with different surface wettability. Nonetheless, air could diffuse through EPDM reducing the working time significantly (Paul and Joseph, 2014). Hirayanagi et al. (2013) investigated a micro thermal diode with an embedded micro glass thermal insulation structure, in which a silicone rubber gasket was used to separate the heating and cooling sections, but its rectification ratio was only up to 1.47. Besides, Wong et al. (2019) studied a water-vapor chamber thermal diode without vacuum, and the thermal rectification ratio was only 1.43. Tsukamoto et al. (2017) proposed a micro thermal diode based on the wettability difference between the top and bottom surfaces without the rubber gasket, in which the thermal rectification ratio was only up to 2.8. Moreover, Traipattanakul et al. (2019) reported a phase change thermal diode with a Teflon gasket (for electric and thermal insulation) using electrostatic-induced coalescing-jumping droplets, which controlled the droplet moving direction by an electric field. However, the electric field makes it difficult to be widely used because of the requirement of power input. Besides, air diffusion through the Teflon gasket could weaken its thermal performance significantly (Peirce 2nd, 1958). It should be noted that the above-mentioned thermal rectifiers can only transport heat from the bottom to top locations with an inclination angle, while they could not work for horizontal heat transfer. Meanwhile, their heat transport distance is generally too short to be used for industrial applications where the heat source and thermal load are generally located in diverse positions. Moreover, the requirement of heat absorption and extraction may vary depending different processes. Hence, existing thermal rectifiers cannot meet the practical end-use requirements.

A horizontal thermal rectifier, which can function without the requirement of height difference between the heat source and the thermal load, overcomes the limitation of the vertical thermal rectifier and makes the thermal device more compact, leading to less investment cost and high working efficiency. Ochi et al. (1996) developed a horizontal thermal diode with PCTFE (Polychlorotrifluoroethylene) adiabatic section to achieve directional heat flow, but its forward thermal conductivity was too low for industrial thermal applications (i.e., 0.67W/(m·K)). Groll

et al. (1979) developed a liquid-trap heat pipe thermal diode for horizontal heat transfer in cryogenic applications, via which the rectification ratio reached 384. However, it worked at a low temperature (−20 °C) and took a long time (20 min) to get this rectification effect. Boreyko et al. (2011) proposed a planar jumping-drop thermal diode that could work horizontally with a maximum rectification ratio of over 100, whereas its forward thermal conductivity was limited.

In this study, we proposed a heat-pipe-based scalable horizontal thermal rectifier with multiple working modes using a copper tube loop having different inner surface wettability in the heating and cooling sections, which performed like a loop heat pipe (Maydanik, 2005) with high forward thermal conductivity. Meanwhile, the proposed thermal rectifier could overcome the drawbacks of the air diffusion through the polymers gaskets (e.g., PTFE, EPDM) due to the metal body. Besides, a valve was incorporated in the adiabatic section, which could tune the working modes with different thermal resistances and rectification ratios with a quick response based on the working situations, and therefore it is of great importance for waste heat recovery, renewable energy harvest, building energy management, etc.

2. Methods

2.1. Working principle

The working principle of the proposed thermal rectifier is illustrated schematically in Fig. 1, in which the superhydrophilic and superhydrophobic sections are positioned vertically. Meanwhile, a wicking layer is introduced on the inner surface of the superhydrophilic section. Hence, when the superhydrophilic section is heated (i.e., forward heating), water evaporates rapidly within the whole superhydrophilic section due to liquid wicking, and the hot vapor flows through the top channel to condense in the superhydrophobic section, which contributes to dropwise condensation enhancing the forward heat transport. On the contrary, evaporation hardly occurs when heating the superhydrophobic section (i.e., reversed heating) and the liquid will be entrapped within the superhydrophilic section to prevent the reversed heat transport. Besides, the valve in the top channel could control the vapor transport within the loop to alter the working mode. Moreover, the heat transport distance could be adjusted by changing the lengths of the top and bottom tubes in the adiabatic section, which makes this device very adaptable for industrial applications. Meanwhile, the connection parts of the tubes are made of metal, which has excellent airtightness for prolonged work. Thus, the proposed thermal rectifier could satisfy various application scenarios for advanced thermal management and energy applications.

2.2. Fabrication of the thermal rectifier

A prototype of the proposed thermal rectifier was constructed with a loop of the copper tube having the inner and outer diameters of 8 mm and 10 mm, respectively. The total length and height of the thermal rectifier including the connectors were 320 mm and 145 mm, respectively. However, the lengths of the heating and cooling sections were both 59 mm, while the central distance between the heating and cooling tubes was 262 mm. To enhance the wicking capability within the superhydrophilic tube, three layers of copper mesh (NO. 300) treated to be superhydrophilic were inserted within the superhydrophilic section. The procedures of the superhydrophilic and superhydrophobic surface treatment are shown in the supplementary file. A T-junction was installed at the bottom channel of the thermal rectifier for vacuuming the copper loop and then injecting working fluid (DI water). The schematic experimental setup is shown in Fig. 2(a). Fig. 2(b) gives the scanning electron microscopic (SEM) image of the superhydrophobic surface, which contributes to dropwise condensation because water droplets cannot attach to it as shown in Video S1 in the supplementary file. Fig. 2(c) denotes the superhydrophilic tube loaded with the superhydrophilic copper mesh, which is used to wick or entrap the liquid water. Figs. 2(d) and (e) present the SEM images of the superhydrophilic copper surface and mesh surface, respectively, which indicate that the superhydrophilic copper and mesh surface are full of nanostructures. The water droplet spreads very fast once it contacts the superhydrophilic copper or mesh surface (see Videos S2 and S3 in supplementary file), which leads to zero contact angle. An electric resistance wire was enwound around the heating tube uniformly as a heater. To measure temperatures at different locations of the thermal rectifier, three K-type thermocouples numbered by T_1, T_2, and T_3 were positioned at the bottom, middle, and top of the superhydrophilic tube, respectively, whereas the other three K-type thermocouples with the number of T_4, T_5, and T_6 were positioned at the bottom, middle and top of the superhydrophobic tube, respectively. Agilent 34970 A was used to record the temperature data with an accuracy of 0.001 °C. Furthermore, the heating and adiabatic sections were insulated by insulation foam to prevent heat dissipation.

The performance of the thermal rectifier was investigated at various heat fluxes from 537 W/m^2 to 3222 W/m^2 (i.e., heating power from 1 W to 6 W) at the heating section when the filling ratio was 30%. Meanwhile, the cooling section was exposed in the ambient environment with a temperature of 23.0 ± 0.5 °C. It should be noted that the filling ratio of 30% was found to give the maximum rectification ratio of this setup based on the preliminary experiments. This is because the liquid water just filled up the bottom tube, which could prevent water evaporation in the superhydrophobic tube at the reversed heating condition. Besides, a small vapor channel could be formed in the bottom tube at the forward heating condition due to the intense evaporation within the superhydrophilic tube, which could improve the vapor circulation through the tube loop to enhance the forward heat transport. The detailed experimental procedures are shown in the supplementary file.

3. Results and discussion

3.1. Temperature distribution of the thermal rectifier

Fig. 3 shows the average temperatures (red line + symbol) of the hotter and cooler sections, and the temperature distributions along the cooling tubes (column) with respect to the heating heat flux under the forward and reversed heating conditions. Both average temperatures of the hotter side (T_h) and cooler side (T_c) increase with the increasing heat flux in the heating section. Fig. 3(a) also denotes that, as the heat flux increases, the difference between T_h and T_c is almost constant (around 15 °C), which means the corresponding thermal resistance decreases. Moreover, the temperature increases along with the height of the cooling tube because the hot vapor flows from the top to the bottom within the cooling tube under forward heating with open control valve. As the tube surface and copper mesh are superhydrophilic within the heating tube, liquid water could wick along the copper tube enhancing the liquid evaporation. Moreover, the dropwise condensation could take place within the cooling tube because of the superhydrophobic surface as denoted in Video S1. Hence, the hot vapor flows upward and downward in the heating and cooling tubes, respectively. As the heat flux increases, the higher heating temperature leads to larger vapor pressure enhancing the vapor transport from the heating tube to

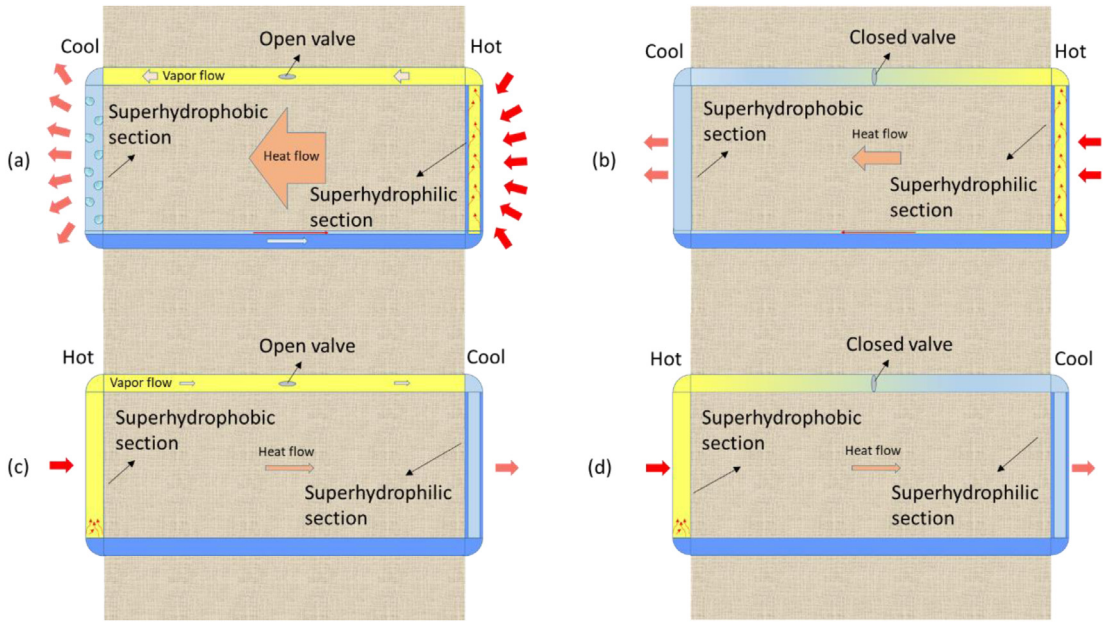

Fig. 1. Schematic diagram of the heat transport mechanisms under (a)–(b) forward heating with open and closed valves, and (c)–(d) reversed heating with open and closed valves.

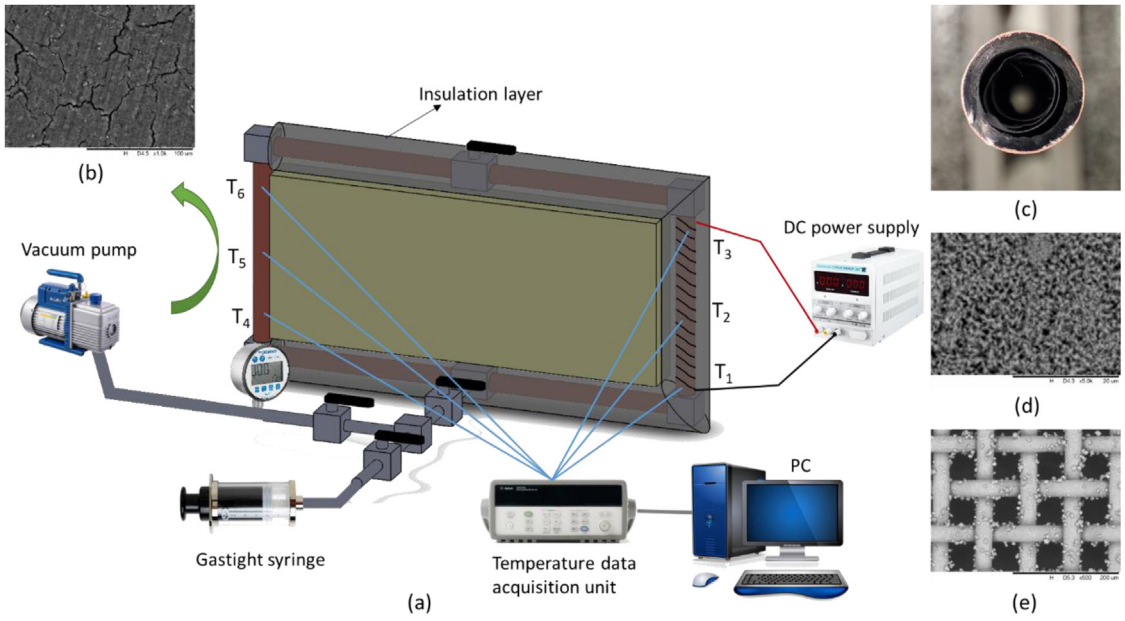

Fig. 2. Schematic chart of the (a) experimental setup, (b) superhydrophobic copper surface (SEM), (c) superhydrophilic copper tube loaded with superhydrophilic mesh (photo), (d) superhydrophilic copper surface (SEM), and (e) superhydrophilic copper mesh (SEM).

the cooling tube, which results in a nearly constant temperature difference between the heating and cooling sections at a large range of heating heat flux. Fig. 3(b) indicates that the difference between T_h and T_c increases with the increasing heat flux under forward heating with closed valve. This is because the closed valve blocked the vapor transport from the heating section to the cooling section via the top channel reducing the heat transfer capability, so that the thermal resistance reduction at higher heat flux is smaller than that with open valve. Hence, the temperature difference between T_h and T_c will be enlarged with the growth of the heating heat flux. Fig. 3(b) also shows that the temperature distribution along the cooling tube is uniform when the heat flux is small (i.e., $q < 1611$ W/m^2), while the bottom temperature is the highest at relatively large heat fluxes ($q \geq 2148$ W/m^2), which is different from the results under forward heating with open valve. The uniform cooling side temperature at a lower heat flux is because the hot vapor cannot transport from the heating section to the cooling section via the top channel and, meanwhile, the evaporation intensity is not sufficient to create a vapor channel at the bottom tube due to the low heat flux. In contrast, at the high heat flux, the large hotter side temperature leads to intense liquid evaporation within the superhydrophilic tube, which is sufficient to produce a narrow channel at the bottom tube for vapor transport as indicated in Fig. 1(b). This results in the higher bottom temperature of the cooling tube and the smaller T_h increasing rate at the heat fluxes from 2148 W/m^2 to 3222 W/m^2 as denoted in Fig. 3(b).

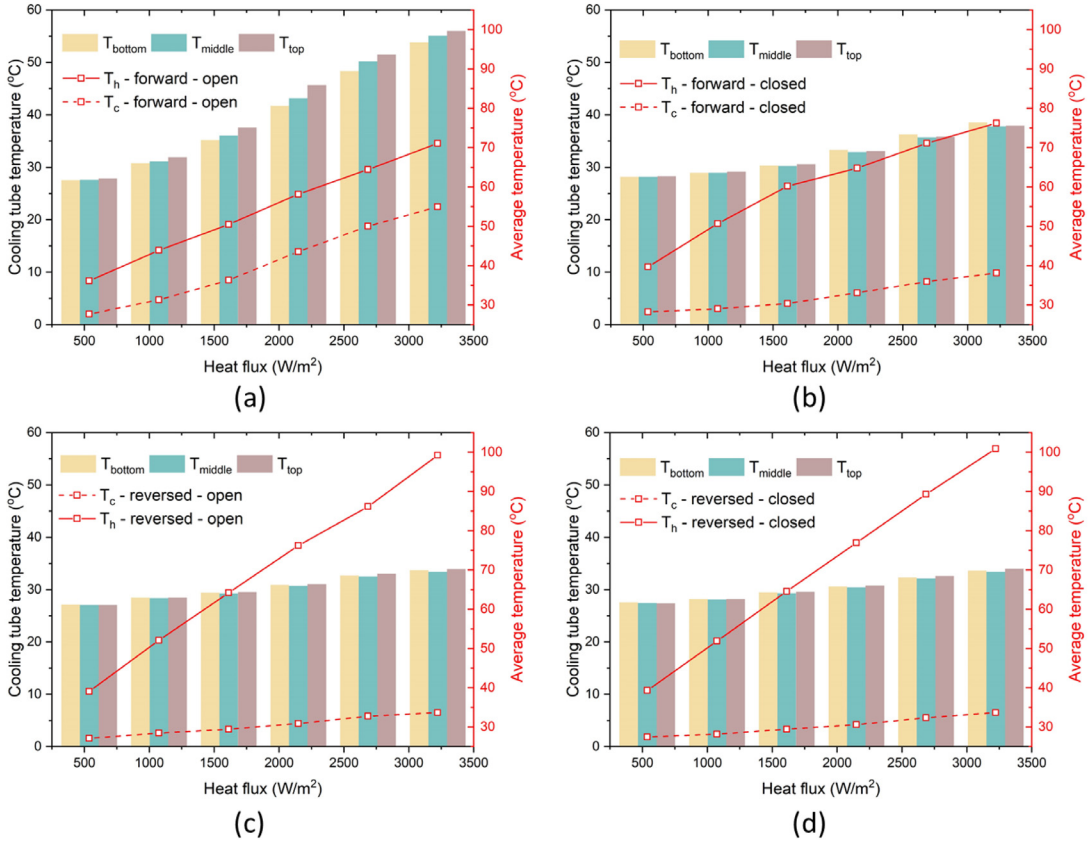

Fig. 3. Average temperatures of the hotter (T_h) and cooler (T_c) sides (red line + symbol), and the temperature distributions from bottom to top of the cooling tube (column) against the heating heat flux: (a) forward heating with open valve; (b) forward heating with closed valve; (c) reversed heating with open valve; (d) reversed heating with closed valve.

Fig. 3(c) depicts that, under the reversed heating with open valve, T_h increases sharply with the increasing heat flux, whereas T_c increases slowly against the heat flux. This is because the superhydrophobic tube cannot wick up liquid water for evaporation, and thus the evaporation only takes place at the bottom of the heating tube as denoted in Fig. 1(c). Hence, the temperature along the whole heating tube soars up due to the lack of evaporative heat dissipation, leading to higher T_h at larger heat flux. Meanwhile, the weak evaporation in the superhydrophobic heating tube also reduces the hot vapor transport from the heating tube to the cooling tube. Besides, the condensed liquid is entrapped within the wicking layer in the superhydrophilic cooling tube as indicated in Fig. 1(c), which not only suppresses the liquid water backflow for evaporation but also hinders the heat transport from the inner vapor to the ambient environment due to the large thermal resistance of the water layer. Consequently, the temperature of the cooling tube (T_c) increases slowly with the increasing heat flux. As a result, the temperature difference between T_h and T_c becomes increasingly greater at larger heat flux. Due to the high temperature in the heating section, heat conduction from the heating tube to the cooling tube through the adiabatic section plays a significant role. Consequently, the temperatures at the top and bottom of the cooling tube (T_{top} and T_{bottom}) are slightly higher than that in the middle position (T_{middle}) as shown in Fig. 3(c). Fig. 3(d) shows that T_h under reversed heating with closed valve is slightly higher than that with open valve in Fig. 3(c). This is because the closed valve blocks the hot vapor transport from the heating section to the cooling section. As no evaporation takes place on the superhydrophobic surface within the heating tube, the evaporation mainly occurs from the water surface in the bottom tube due to heat conduction, and thus the evaporation intensity is very small. Hence, the valve status has a weak effect on the heat transport process. As a result, the average cooling temperatures (T_c) and the temperature distributions along the cooling tube under the reversed heating with open and closed valves are similar to each other as denoted in Figs. 3(c) and (d).

3.2. Rectification effect for horizontal heat transport

In this study, the average temperatures of the heating and cooling sections (T_h and T_c) were used as the heating and cooling temperatures, respectively, to determine the thermal resistance. Hence, the thermal resistance of the thermal rectifier could be calculated by Mahdavi et al. (2018)

$$R = \frac{T_h - T_c}{q \cdot S} \tag{1}$$

where T_h and T_c are the average temperatures of the heating and cooling sections, respectively; q is the heat flux from the heating tube surface; S is the surface area of the vertical heating tube. Besides, the equivalent thermal conductivity could be obtained by Mahdavi et al. (2018) $k = L/(A \cdot R)$, where L is the distance between the heating and cooling sections, and A is the total cross-section area of the top and bottom tubes. Furthermore, in this study, the rectification ratio of the thermal rectifier is determined by the thermal resistance ratio between the reversed and forward heating conditions, which characterizes the heat transport capability between forward heating and reversed heating. Thus, the rectification ratio (φ) could be obtained by Hirayanagi et al. (2013)

$$\varphi = \frac{R_r}{R_f} \tag{2}$$

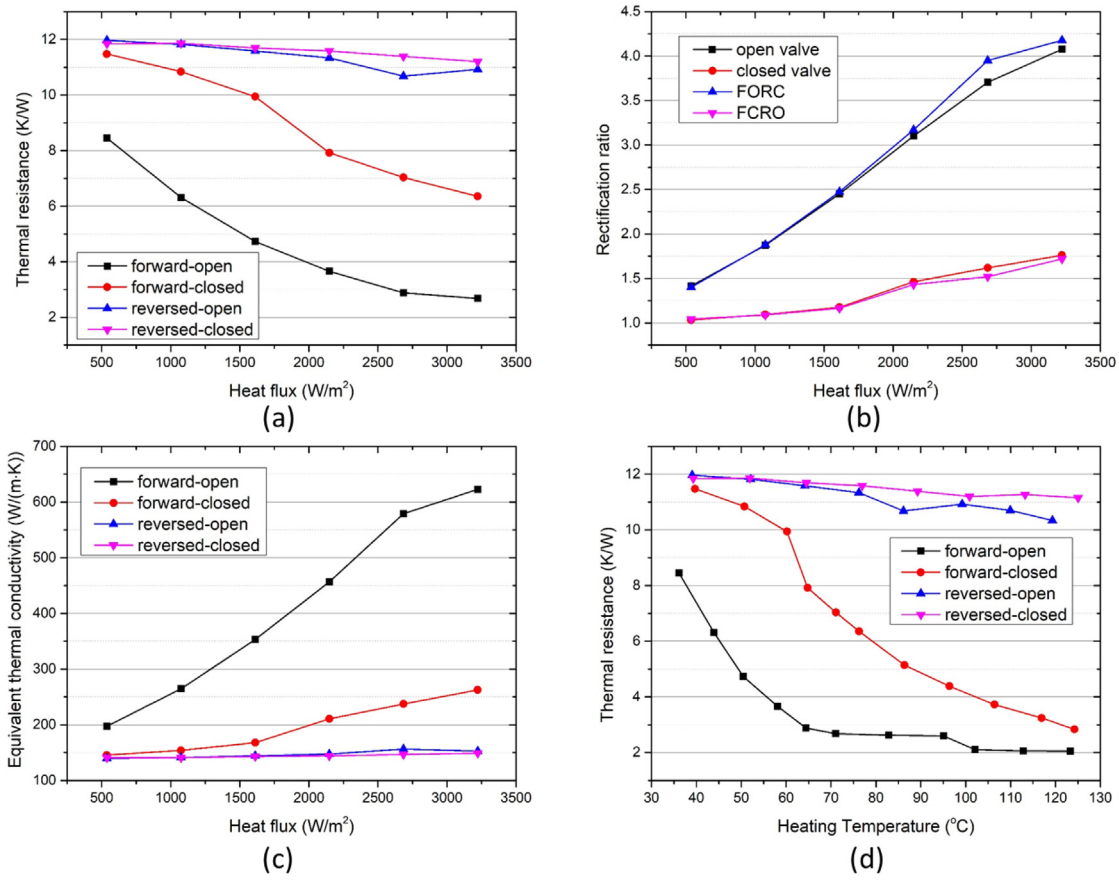

Fig. 4. Thermal performance of the thermal rectifier: (a) thermal resistance, (b) rectification ratio (FORC: forward-open valve & reversed-closed valve; FCRO: forward-closed valve & reversed-open valve), and (c) equivalent thermal conductivity versus heating heat flux, and (d) the thermal resistance against the hotter side temperature.

where R_r and R_f are the thermal resistances during reversed and forward heating conditions, respectively.

Fig. 4 shows the thermal performance of the proposed thermal rectifier for horizontal heat transport under different working modes with respect to the heating heat flux and the hotter side temperature. Fig. 4(a) denotes the thermal resistance under forward and reversed heating conditions with open and closed valves, which indicates that the thermal resistance reduces with the increasing heat flux. Moreover, the forward heating thermal resistance is lower than the reversed heating thermal resistance, which is because the superhydrophilic and superhydrophobic tube surfaces under forward heating conditions significantly contribute to the evaporative and condensation heat transfer, respectively. Meanwhile, the open valve is also beneficial to reducing the thermal resistance due to the vapor exchange enhancement between the heating and cooling sections. Consequently, by changing the valve status, the heating mode could be varied with different thermal resistances to meet the complex requirement in practical applications, which also could work as a thermal valve to control the heat transport capability. It is interesting to note that the valve has a larger effect under forward heating than that under reversed heating. This is because forward heating generates much more vapor in the superhydrophilic tube so that the vapor blockage induced by the closed valve could impair heat transport significantly. In contrast, the vapor generation in the superhydrophobic tube is very small during reversed heating, and thus whether the valve is closed or open has little effect on the heat transfer from the hotter section to the cooler section. Meanwhile, the forward heating with closed valve has smaller thermal resistance than that under reversed heating with open valve because of the vapor transfer from the bottom tube as indicated in Fig. 1(b).

Fig. 4(b) shows the rectification ratios of the thermal rectifier under open valve, closed valve, forward heating with open valve & reversed heating with closed valve (FORC), and forward heating with closed valve & reversed heating with open valve (FCRO). The rectification ratios are all greater than 1 and they increase with the increasing heating heat flux. Furthermore, the rectification ratios under forward heating with open valve are larger than those under forward heating with closed valve. Hence, the thermal rectifier could work in multiple modes with different rectification ratios controlled by the valve to satisfy the various end-use requirement. The highest rectification ratio could reach 4.18 for FORC, whereas the thermal rectifier with open valve in both forward and reversed heating still has a rectification ratio up to 4.07. However, when a smaller rectification ratio is required in some applications, the working mode with closed valve or FCRO may be adopted as their rectification ratios range from 1.03 to 1.76. Furthermore, preliminary experiments have indicated that the maximum rectification ratio even increases with longer heat transport distance (i.e., longer bottom and top tubes).

Fig. 4(c) depicts the equivalent thermal conductivity of the thermal rectifier at different working modes. The highest equivalent thermal conductivity is up to 623 W/(m·K) under forward heating with open valve, which is sufficiently high for waste heat recovery in many industrial scenarios. On the contrary, the equivalent thermal conductivity under reversed heating is only about 140 W/(m·K), which is much smaller than the thermal conductivity of copper. Fig. 4(d) describes the thermal resistance of the thermal rectifier under different working modes with respect

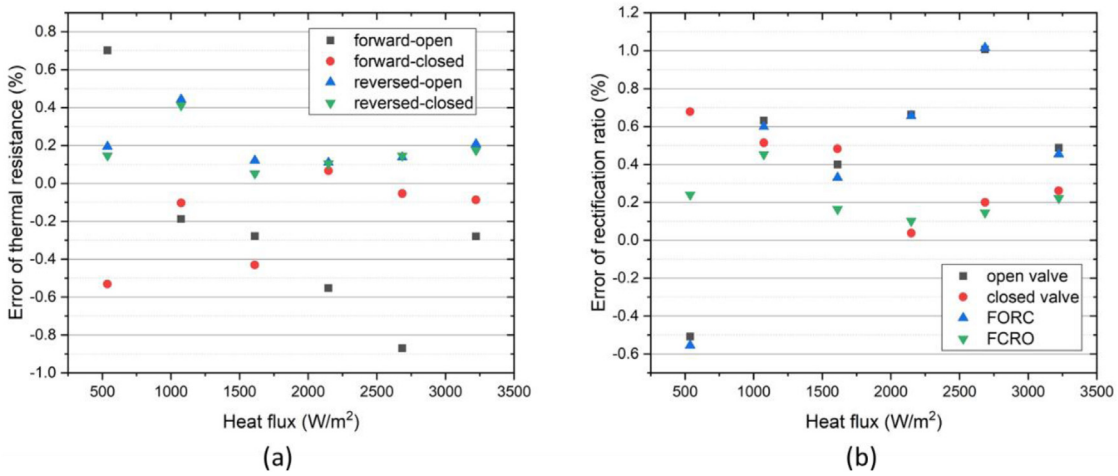

Fig. 5. Measurement error of (a) the thermal resistance and (b) the rectification ratio.

to the hotter side temperature, while the cooler side is exposed in the ambient air, which shows that the thermal resistance is lower at higher hotter side temperatures. In practical applications, the hot side temperature at forwarding heating is generally higher than that at the reversed heating. Consequently, the rectification effect could perform much better in real applications, and the maximum rectification ratio could reach about 5.78 when the hotter side temperatures at the forward and reversed heating conditions are about 123 °C and 52 °C, respectively.

3.3. Uncertainty analysis

According to Eq. (1), the thermal resistance of the thermal rectifier could be obtained by

$$R = \frac{T_h - T_c}{Q} \tag{3}$$

where Q is heating power ($Q = qS$). Hence, the measurement error (ε_R) of the thermal resistance could be calculated by Kang et al. (2017) and Taylor (1997)

$$\varepsilon_R = \frac{\Delta R}{R} = \frac{1}{R}\left(\frac{\Delta T_h}{Q} - \frac{\Delta T_c}{Q} - \frac{T_h - T_c}{Q^2}\Delta Q\right) \tag{4}$$

where ΔR, ΔT_h, ΔT_c and ΔQ are the measurement uncertainties of thermal resistance, hot side temperature, cold side temperature, and heat power, respectively. The measurement uncertainty of the thermal resistance is induced by the temperature uncertainty and the heat power uncertainty. The temperature uncertainty could be regarded as the standard deviation of the temperature data during the experimental process, and the heat power uncertainty is calculated by the difference between the actual heat power and the set heat power. Besides, according to Eq. (2), the measurement error of the rectification ratio (ε_φ) could be derived by

$$\varepsilon_\varphi = \frac{\Delta\varphi}{\varphi} = \frac{1}{\varphi}\left(\frac{1}{R_f}\Delta R_r - \frac{R_r}{R_f^2}\Delta R_f\right) \tag{5}$$

where $\Delta\varphi$, ΔR_f, and ΔR_r are the measurement uncertainties of the rectification ratio, forward thermal resistance and reversed thermal resistance, respectively. As a result, the measurement error of the thermal resistance and rectification ratio could be obtained based on Eqs. (4) and (5), which are depicted in Fig. 5. Fig. 5(a) shows the measurement error of thermal resistance is within 1%, whereas the maximum error of the rectification ratio is only about 1%. Therefore, the measurement error of this experiment is acceptable.

4. Concluding remarks

In this study, we proposed a heat-pipe-based thermal rectifier with multiple working modes for the control of horizontal heat transport. The thermal rectifier is composed of a copper tube loop having a superhydrophilic section filled with superhydrophilic mesh, and a superhydrophobic section. Meanwhile, a valve is incorporated in the vapor channel to control the hot vapor exchange between the heating and cooling sections. The thermal rectification effect is achieved by the differences of the superhydrophilic and superhydrophobic sections in surface evaporation/condensation and wicking characteristics, when they are exposed to heating or cooling. Experiments with such a thermal rectifier showed that a maximum thermal rectification ratio of 4.18 can be reached under constant heat flux in the case of forward heating with open valve and reversed heating with closed valve. In practical applications, a maximum rectification ratio of 5.78 even can be reached. Moreover, the maximum forward thermal conductivity was up to 623 W/(m· K), which could be used for efficient thermal management and waste heat recovery. Furthermore, the thermal resistance and rectification ratio can be altered by the status of the valve to adapt to the complex end-use applications. The proposed thermal rectifier can be easily scaled up for industrial applications by simply varying the length of the tube loop. Besides, the valve could work as a thermal valve to control the heat flux from the hotter side to the cooler side during forward heating mode. Therefore, it has highly promising potential for advanced thermal energy management, such as waste heat recovery, solar energy harvest, and building energy management, which could contribute to energy saving, pollution reduction, and the reduction of greenhouse gas emissions.

CRediT authorship contribution statement

Zhanxiao Kang: Conceptualization, Methodology, Data curation, Writing – original draft. **Jintu Fan:** Conceptualization, Supervision, Writing – review & editing, Funding acquisition.

Declaration of competing interest

The authors declare that they have no known competing financial interests or personal relationships that could have appeared to influence the work reported in this paper.

Acknowledgments

The financial support from the Hong Kong Polytechnic University (G-YW5D and 99ZZ) is gratefully acknowledged. The work is also supported by PolyU AoEC Project: Wearable Technology for Personal Thermal Management (Project No: ZE1H).

Appendix A. Supplementary data

Supplementary material related to this article can be found online at https://doi.org/10.1016/j.egyr.2022.03.042.

References

Azad, E., 2008. Theoretical and experimental investigation of heat pipe solar collector. Exp. Therm Fluid Sci. 32, 1666–1672.
Boreyko, J.B., Zhao, Y., Chen, C.-H., 2011. Planar jumping-drop thermal diodes. Appl. Phys. Lett. 99.
Chen, K., Chailapo, P., Chung, W., Kim, S., Lee, K.J., 1998. The dynamic behavior of a bayonet-type thermal diode. Sol. Energy 64, 257–263.
Crane, D.T., Jackson, G.S., 2004. Optimization of cross flow heat exchangers for thermoelectric waste heat recovery. Energy Convers. Manage. 45, 1565–1582.
Edalatpour, M., Murphy, K.R., Mukherjee, R., Boreyko, J.B., 2020. Bridging-droplet thermal diodes. Adv. Funct. Mater. 30.
Garimella, S., 2012. Low-grade waste heat recovery for simultaneous chilled and hot water generation. Appl. Therm. Eng. 42, 191–198.
Groll, M., Munzel, W.D., Supper, W., Savage, C.J., 1979. Development of a liquid-trap heat pipe thermal diode. J. Spacecr. Rockets 16, 195–202.
Hamaoui, G., Horny, N., Gomez-Heredia, C.L., Ramirez-Rincon, J.A., Ordonez-Miranda, J., Champeaux, C., et al., 2019. Thermophysical characterisation of VO2 thin films hysteresis and its application in thermal rectification. Sci. Rep. 9, 8728.
Hervás-Blasco, E., Navarro-Peris, E., Corberán, J.M., 2019. Optimal design and operation of a central domestic hot water heat pump system for a group of dwellings employing low temperature waste heat as a source. Energy 188.
Hirayanagi, T., Tsukamoto, T., Esashi, M., Tanaka, S., 2013. Micro thermal diode with glass thermal insulation structure embedded in vapor chamber. J. Phys. Conf. Ser. 476.
Hu, M., Keblinski, P., Li, B., 2008. Thermal rectification at silicon-amorphous polyethylene interface. Appl. Phys. Lett. 92.
Hu, B., Yang, L., Zhang, Y., 2006. Asymmetric heat conduction in nonlinear lattices. Phys. Rev. Lett. 97, 124302.
Jouhara, H., Khordehgah, N., Almahmoud, S., Delpech, B., Chauhan, A., Tassou, S.A., 2018. Waste heat recovery technologies and applications. Thermal Science and Engineering Progress 6, 268–289.
Kang, Z., Shou, D., Fan, J., 2021. Numerical study of a novel single-loop pulsating heat pipe with separating walls within the flow channel. Appl. Therm. Eng. 196.
Kang, Z., Wang, L., 2018. Boiling heat transfer on surfaces with 3D-printing microstructures. Exp. Therm Fluid Sci. 93, 165–170.
Kang, Z., Zhu, P., Gui, D., Wang, L., 2017. A method for predicting thermal waves in dual-phase-lag heat conduction. Int. J. Heat Mass Transfer 115, 250–257.
Liu, D., Tang, G.-F., Zhao, F.-Y., Wang, H.-Q., 2006. Modeling and experimental investigation of looped separate heat pipe as waste heat recovery facility. Appl. Therm. Eng. 26, 2433–2441.
Mahajan, G., Thompson, S.M., Cho, H., 2017. Energy and cost savings potential of oscillating heat pipes for waste heat recovery ventilation. Energy Rep. 3, 46–53.
Mahdavi, M., Tiari, S., De Schampheleire, S., Qiu, S., 2018. Experimental study of the thermal characteristics of a heat pipe. Exp. Therm Fluid Sci. 93, 292–304.
Mahmoudi, A., Fazli, M., Morad, M.R., 2018. A recent review of waste heat recovery by Organic Rankine Cycle. Appl. Therm. Eng. 143, 660–675.
Maydanik, Y.F., 2005. Loop heat pipes. Appl. Therm. Eng. 25, 635–657.
Ochi, T., Ogushi, T., Aoki, R., 1996. Development of a heat-pipe thermal diode and its heat transport performance. Jsme Int. J. B-Fluid T. 39, 419–425.
Ordonez-Miranda, J., Hill, J.M., Joulain, K., Ezzahri, Y., Drevillon, J., 2018. Conductive thermal diode based on the thermal hysteresis of VO2 and nitinol. J. Appl. Phys. 123.
Pal, S., Puri, I.K., 2014. Thermal rectification in a polymer-functionalized single-wall carbon nanotube. Nanotechnology 25, 345401.
Paul, P., Joseph, R., 2014. EPDM/CIIR Blends: rheology, air permeability, thermal stability and thermal diffusivity. Int. J. Sci. Environ. Technol. 3, 1359–1370.
Pei, W., Zhang, M., Li, S., Lai, Y., Dong, Y., Jin, L., 2019. Laboratory investigation of the efficiency optimization of an inclined two-phase closed thermosyphon in ambient cool energy utilization. Renew. Energy 133, 1178–1187.
Peirce 2nd, E.C., 1958. Diffusion of oxygen and carbon dioxide through teflon membranes. AMA Arch. Surg. 77, 938–943.
Pugsley, A., Zacharopoulos, A., Deb Mondol, J., Smyth, M., 2019. Theoretical and experimental analysis of a horizontal planar Liquid-Vapour Thermal Diode (PLVTD). Int. J. Heat Mass Transfer 144.
Rivera, C.O., Rivera, W., 2003. Modeling of an intermittent solar absorption refrigeration system operating with ammonia-lithium nitrate mixture. Sol. Energy Mater. Sol. Cells 76, 417–427.
Shrestha, R., Luan, Y., Luo, X., Shin, S., Zhang, T., Smith, P., et al., 2020. Dual-mode solid-state thermal rectification. Nature Commun. 11, 4346.
Susheela, N., Sharp, M.K., 2001. Heat pipe augmented passive solar system for heating of buildings. J. Energy Eng. 127, 18–36.
Takeuchi, T., 2014. Very large thermal rectification in bulk composites consisting partly of icosahedral quasicrystals. Sci. Technol. Adv. Mater. 15, 064801.
Taylor, J., 1997. Introduction to error analysis, the study of uncertainties in physical measurements.
Traipattanakul, B., Tso, C.Y., Chao, C.Y.H., 2019. A phase-change thermal diode using electrostatic-induced coalescing-jumping droplets. Int. J. Heat Mass Transfer 135, 294–304.
Tsukamoto, T., Hirayanagi, T., Tanaka, S., 2017. Micro thermal diode with glass thermal insulation structure embedded in a vapor chamber. J. Micromech. Microeng. 27.
Varga, S., Oliveira, A.C., Afonso, C.F., 2002. Characterisation of thermal diode panels for use in the cooling season in buildings. Energy Build. 34, 227–235.
Villeneuve, T., Boudreau, M., Dumas, G., 2017. The thermal diode and insulating potentials of a vertical stack of parallelogrammic air-filled enclosures. Int. J. Heat Mass Transfer 108, 2060–2071.
Wang, D.C., Wu, J.Y., 2005. Influence of intermittent heat source on adsorption ice maker using waste heat. Energy Convers. Manage. 46, 985–998.
Wong, M.Y., Traipattanakul, B., Tso, C.Y., Chao, C.Y.H., Qiu, H., 2019. Experimental and theoretical study of a water-vapor chamber thermal diode. Int. J. Heat Mass Transfer 138, 173–183.
Zhang, T., Luo, T., 2015. Giant thermal rectification from polyethylene nanofiber thermal diodes. Small 11, 4657–4665.
Zhang, T., Yan, Z.W., Wang, L.Y., Zheng, W.J., Su, Y.H., 2020. Comparative study on the annual performance between loop thermosyphon solar water heating system and conventional solar water heating system. Sol. Energy 197, 433–442.